JOURNAL OF GUIDANCE, CONTROL, AND DYNAMICS
Vol. 33, No. 6, November–December 2010

Robust Adaptive Design for Aerial Vehicles with State-Limiting Constraints

Eugene Lavretsky* and Ross Gadient†
The Boeing Company, Huntington Beach, California 92647

DOI: 10.2514/1.50101

This paper presents robust adaptive augmentation design for a class of second-order uncertain nonlinear cascaded systems. These dynamics generalize the models that are often used for the design of inner-loop flight controllers for aerial vehicles. The proposed control architecture augments a baseline dynamic inversion controller with a direct adaptive component and a state-limiting component. While the adaptive augmentation is designed to maintain tracking performance in the presence of the system uncertainties, the state-limiting component protects the system trajectories from leaving an allowable subset in the system state space. The proposed design is applied to construct angle-of-attack command-tracking system for short-period dynamics of a fixed-wing aircraft, with simulation results presented.

I. Introduction

CONSIDER second-order uncertain dynamical systems in the cascaded form:

$$\begin{cases} \dot{x}_1 = F_1^0(x_1, z) + B_1 x_2 + f_1(x_1, z) \\ \dot{x}_2 = F_2^0(x_1, x_2, z) + \dot{x}_2^{\text{cmd}} + f_2(x_1, x_2, z) \end{cases} \tag{1}$$

where $x = (x_1 \quad x_2)^T$ is the system state vector, z is the known bounded external signal, (F_0^1, F_0^2) are known state-dependent functions, B_1 is a known nonzero constant, $\dot{x}_2^{\text{cmd}}$ is the system control input, and (f_1, f_2) are unknown continuously differentiable functions that represent the system uncertainties.

The control objective is bounded tracking in the presence of the system uncertainties (f_1, f_2). Specifically, the control goal is to design the control input $\dot{x}_2^{\text{cmd}}$ so that the system first state component x_1 tracks any given bounded time-varying command $x_1^{\text{cmd}}(t)$, in the presence of the system uncertainties, while keeping all the signals in the closed-loop system bounded, uniformly in time.

Interest in considering this particular class of systems stems from flight control related applications, where inner-loop controllers for a fixed-wing aircraft are often designed based on the so-called simplified models [1–4]. The latter are given in the form of Eq. (1) and represent the aircraft decoupled fast responses in pitch, roll, and yaw axes. This paper expands and refines the concepts first presented in [5] and, in addition, demonstrates the developed technology on a relevant simulation example using representative flight dynamics models.

The *first control challenge* addressed in this paper is the design of an inner-loop controller that maintains system tracking performance in the presence of uncertain aerodynamic effects, control failures, and unknown environmental disturbances. This is accomplished using flight-proven adaptive design methods from [1,3].

Moreover, an aircraft flight controller must keep the vehicle dynamics in a prespecified region of the corresponding state space. This region is often referred to as the operational flight envelope. For example, an angle-of-attack (AOA) command-tracking controller must include an AOA protection system (often called the AOA Limiter), whose purpose is to maintain the aircraft AOA within a prespecified range, outside of which a loss of control is expected. In essence, such an AOA controller would have to blend the two subsystems, the AOA tracker and the AOA limiter, with seamless transitions between the two controllers, while preserving closed-loop stability at all times. Combining these two subsystems into a single inner-loop controller, while using theoretically justified design methods with performance and stability guarantees, constitutes the *second control challenge*. To address the latter, this paper proposes and employs a modification to the state-limiting (SL) design idea originally developed in [6].

Furthermore, in real-world flight control applications, an inner-loop system must often provide adequate damping in the presence of high order dynamics, such as the system structural modes, as well as other unmodeled effects. Toward that end, the *third control challenge* consists of adding damping to the system dynamics at low frequencies only, and without exciting the high-frequency modes. The proposed robust adaptive controller addresses and solves all three of the control challenges.

The rest of the paper is organized as follows. Section II presents the proposed robust adaptive control architecture. Online representation of the system uncertainties is discussed in Sec. III. Sufficient conditions that guarantee closed-loop stability and bounded tracking are stated in Sec. IV. Based on these results, Sec. V contains AOA command-tracking design, with flight-envelope protection logic, and adaptive damping. This controller is constructed for short-period dynamics of a fixed-wing aircraft, and simulation examples are presented. The paper ends with conclusions that are given in Sec. VI.

II. Model Reference Control Architecture

This paper will employ a model-reference-based control design framework. The reference model is chosen to be second-order, with the desired damping ratio ξ and the natural frequency ω:

$$x_1^m = \left[\frac{\omega^2}{s^2 + 2\xi\omega s + \omega^2}\right] x_1^{\text{cmd}} \tag{2}$$

This model is driven by a bounded, possibly time-varying, reference command x_1^{cmd}. Alternatively, Eq. (2) can be expressed in the state-space form:

$$\begin{pmatrix} \dot{x}_1^m \\ \ddot{x}_1^m \end{pmatrix} = \begin{pmatrix} 0 & 1 \\ -\omega^2 & -2\xi\omega \end{pmatrix} \begin{pmatrix} x_1^m \\ \dot{x}_1^m \end{pmatrix} + \begin{pmatrix} 0 \\ \omega^2 \end{pmatrix} x_1^{\text{cmd}} \tag{3}$$

Differentiating the first state component in Eq. (1) yields

$$\ddot{x}_1 = \frac{\partial F_1^0}{\partial x_1}\dot{x}_1 + \frac{\partial F_1^0}{\partial z}\dot{z} + B_1\dot{x}_2 + \frac{\partial f_1}{\partial x_1}\dot{x}_1 + \frac{\partial f_1}{\partial z}\dot{z} \tag{4}$$

Received 29 March 2010; revision received 12 July 2010; accepted for publication 16 July 2010.

*Senior Technical Fellow. Associate Fellow AIAA.
†Engineer. Senior Member AIAA.

Substituting the first equation from Eq. (1) into Eq. (4) results in

$$\ddot{x}_1 = \underbrace{\left[\frac{\partial F_1^0}{\partial x_1}(F_1^0 + B_1 x_2) + \frac{\partial F_1^0}{\partial z}\dot{z} + B_1 F_2^0\right]}_{f(x_1,x_2,z,\dot{z})} + B_1 \dot{x}_2^{\text{cmd}} + \underbrace{\left[\frac{\partial F_1^0}{\partial x_1} f_1 + \frac{\partial f_1}{\partial x_1}(F_1^0 + B_1 x_2 + f_1) + \frac{\partial f_1}{\partial z}\dot{z} + B_1 f_2\right]}_{d(x_1,x_2,z,\dot{z})} \quad (5)$$

or, equivalently

$$\ddot{x}_1 = f(x_1, x_2, z, \dot{z}) + B_1 \dot{x}_2^{\text{cmd}} + d(x_1, x_2, z, \dot{z}) \quad (6)$$

One may immediately note that in Eq. (6) the function $f(x_1, x_2, z, \dot{z})$ and the constant B_1 are known, while $d(x_1, x_2, z, \dot{z})$ represents the unknown system uncertainty.

For the system (6), consider a dynamic-inversion-based controller (baseline system) in the form

$$\dot{x}_2^{\text{cmd}} = B_1^{-1}\left(\ddot{x}_1^m - f - K_D(\hat{\dot{x}}_1 - \dot{x}_1^m) - K_P(x_1 - x_1^m) - K_I\left(\frac{x_1(t) - x_1^m(t)}{s}\right) - v\right) \quad (7)$$

where

$$\frac{x_1(t) - x_1^m(t)}{s} \triangleq \int_0^t (x_1(\tau) - x_1^m(\tau))\,\mathrm{d}\tau \quad (8)$$

is the integrated model tracking error, and

$$\hat{\dot{x}}_1 = F_1^0(x_1, z) + B_1 x_2 \quad (9)$$

is the estimated/predicted first state derivative. Also in Eq. (7), v denotes an augmentation component that will be defined later on, via Eq. (12). Let $e_1 = x_1 - x_1^m$ be the reference model tracking-error signal. Substituting Eq. (7) into Eq. (6) results in the closed-loop tracking-error dynamics:

$$\ddot{e}_1 = -K_D\dot{e}_1 - K_P e_1 - K_I\int_0^t e_1(\tau)\,\mathrm{d}\tau + \underbrace{[d - K_D f_1]}_{D(x_1,x_2,z,\dot{z})} - v \quad (10)$$

Introduce the aggregate state $\bar{x} = (x_1 \quad x_2 \quad z \quad \dot{z})^T$. Then Eq. (10) can be written as

$$\ddot{e}_1 = -K_D\dot{e}_1 - K_P e_1 - K_I\int_0^t e_1(\tau)\,\mathrm{d}\tau + D(\bar{x}) - v \quad (11)$$

At this time, control signal v is defined to dominate the system uncertainties online:

$$v \triangleq (1 - \bar{\gamma}(\bar{x}))\hat{D}(\bar{x}) + \bar{\gamma}(\bar{x})v_{sl} + w_{ad} \quad (12)$$

where $\hat{D}(\bar{x}) = \hat{D}(x_1, x_2, z, \dot{z})$ is the online adaptive estimate, w_{ad} is the so-called adaptive damping term to be defined later using a rate lead-lag filter, and v_{sl} represents the SL component (i.e., the state limiter) of the control law. In addition, $\bar{\gamma}(\bar{x})$ is the modulation function. This is a continuous state-dependent map, which allows the controller (12) to smoothly transition between the state limiting and the adaptive modes of operation. Construction of the modulation function is based on [6], and its design is presented below.

Let Ω represent a compact region of representation for the adaptive component $\hat{D}$, and let $\Omega_\delta \subset \Omega$ be its compact subset. The state-dependent modulation function $\bar{\gamma}(\bar{x})$ is defined as

$$\bar{\gamma}(\bar{x}) = \begin{cases} 0, & \bar{x} \in \Omega_\delta \\ 1, & \bar{x} \notin \Omega \\ 0 < \bar{\gamma} < 1, & \bar{x} \in \Omega - \Omega_\delta \end{cases} \quad (13)$$

It provides *continuous* transition from the adaptive component $\hat{D}$ in Eq. (12) to the SL component v_{sl}, if and when the vector $\bar{x}$ leaves the subset Ω_δ, but before it reaches the boundary of Ω. The sufficiently small parameter δ defines the width of the annulus region $\Omega - \Omega_\delta$. Graphical representation of the modulation function is shown in Fig. 1. Specific examples of the modulation function will be presented in Sec. V.

Remark 1: Consider the baseline case without the system uncertainty [that is, $D(\bar{x}) = 0$] and without the augmentation component v. The system closed-loop tracking-error dynamics are

$$\ddot{e}_1 = -K_D\dot{e}_1 - K_P e_1 - K_I\int_0^t e_1(\tau)\,\mathrm{d}\tau \quad (14)$$

This system exhibits the classic proportional–integral derivative (PID) architecture.

The main goal of the adaptive component in Eq. (12) is to dominate the uncertainty $D(\bar{x})$ in Eq. (10) by using its online estimated value $\hat{D}(\bar{x})$. With Eq. (12), the tracking-error dynamics take the form

$$\ddot{e}_1 = -K_D\dot{e}_1 - K_P e_1 - K_I\int_0^t e_1(\tau)\,\mathrm{d}\tau - (1 - \bar{\gamma})\underbrace{(\hat{D} - D)}_{e_D} - \bar{\gamma}(v_{sl} - D) - w_{ad} \quad (15)$$

where e_D is the uncertainty estimation error. Detailed design of the SL component v_{sl} will be presented later in the paper.

Using the pole placement method [4], baseline PID feedback gains are chosen to enforce the desired second-order dynamics (2), augmented by the integrated tracking error. It is easy to show that the corresponding feedback gains are

$$K_D = 2\xi\omega + k_1, \qquad K_P = \omega(\omega + 2\xi k_1), \qquad K_I = \omega^2 k_1 \quad (16)$$

Substituting Eq. (16) into Eq. (15) yields

$$\ddot{e}_1 = -(2\xi\omega + k_1)\dot{e}_1 - \omega(\omega + 2\xi k_1)e_1 - \omega^2 k_1\int_0^t e_1(\tau)\,\mathrm{d}\tau - (1 - \bar{\gamma})e_D - \bar{\gamma}(v_{sl} - D) - w_{ad} \quad (17)$$

Regrouping the terms in Eq. (17) results in

$$\ddot{e}_1 + k_1\dot{e}_1 = -2\xi\omega(\dot{e}_1 + k_1 e_1) - \omega^2\left(e_1 + k_1\int_0^t e_1(\tau)\,\mathrm{d}\tau\right) - (1 - \bar{\gamma})e_D - \bar{\gamma}(v_{sl} - D) - w_{ad} \quad (18)$$

Introduce the filtered tracking error:

$$e_1^f = e_1 + k_1\int_0^t e_1(\tau)\,\mathrm{d}\tau \quad (19)$$

Using Eqs. (18) and (19), the filtered tracking-error dynamics can be written as

$$\ddot{e}_1^f = -2\xi\omega\dot{e}_1^f - \omega^2 e_1^f - (1 - \bar{\gamma})e_D - \bar{\gamma}(v_{sl} - D) - w_{ad} \quad (20)$$

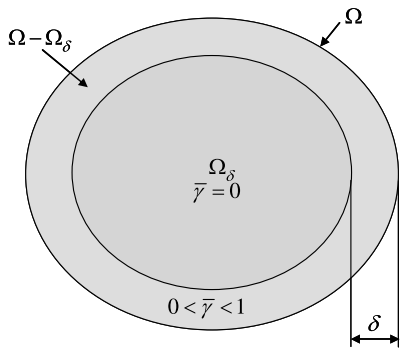

Fig. 1 Modulation function sets.

As seen from Eq. (20), the term $2\xi\omega\dot{e}_1^f$ provides baseline damping to the filtered error dynamics. Often, in real-world applications, the value of the baseline damping term is optimized such that the maximum possible damping is achieved in the presence of high order dynamics, such as the system structural modes, or any other unmodeled effects. To add extra damping, without exciting the high-frequency modes, the former is introduced into the system at low frequencies only. Toward this end, define

$$\eta = \left(\frac{a}{s+a}\right)\dot{e}_1^f = \left(\frac{sa}{s+a}\right)e_1^f \tag{21}$$

and choose the adaptive damping term as

$$w_{ad} = (K_D^f + \hat{k}_D^f)\eta \tag{22}$$

where K_D^f represents the baseline damping gain, $\hat{k}_D^f$ is the adaptive incremental damping gain, and $a > 0$ is the desired crossover frequency, above which the incremental damping must resort back to its baseline value. Relation (22) can be written in the state-space form:

$$\dot{\eta} = -a(\eta - \dot{e}_1^f) \tag{23}$$

Augmenting the error dynamics (20) with Eq. (23), the system extended error dynamics become

$$\underbrace{\begin{pmatrix} \dot{e}_1^f \\ \ddot{e}_1^f \\ \dot{\eta} \end{pmatrix}}_{\dot{e}_f} = \underbrace{\begin{pmatrix} 0 & 1 & 0 \\ -\omega^2 & -2\xi\omega & -K_D^f \\ 0 & a & -a \end{pmatrix}}_{A_{\text{ref}}} \underbrace{\begin{pmatrix} e_1^f \\ \dot{e}_1^f \\ \eta \end{pmatrix}}_{e_f} - \underbrace{\begin{pmatrix} 0 \\ 1 \\ 0 \end{pmatrix}}_{b_{\text{ref}}} ((1-\bar{\gamma})e_D + \bar{\gamma}(v_{sl} - D) + \hat{k}_D^f \eta) \tag{24}$$

where $e_f = (\, e_1^f \quad \dot{e}_1^f \quad \eta\,)^T$ represents the extended filtered tracking-error vector. Next, conditions must be found such that the matrix A_{ref} becomes Hurwitz. The matrix characteristic polynomial is

$$\det(\lambda I - A_{\text{ref}}) = \begin{vmatrix} \lambda & -1 & 0 \\ \omega^2 & \lambda + 2\xi\omega & K_D^f \\ 0 & -a & \lambda + a \end{vmatrix} = \lambda^3 + \lambda^2((2\xi\omega + K_D^f)a + \omega^2) + \omega^2 a \tag{25}$$

For the characteristic polynomial in Eq. (25) to have all its roots in the left half-plane, it is sufficient to impose the following relations:

$$\begin{aligned} &1)\colon a > 0 \qquad 2)\colon K_D^f > -2\xi\omega - \frac{\omega^2}{a} \\ &3)\colon \omega^2 a < (2\xi\omega a + K_D^f a + \omega^2)(2\xi\omega + a) \end{aligned} \tag{26}$$

Remark 2: The first inequality in Eq. (26) is already satisfied, since a defines the desired crossover frequency for the rate filter in Eq. (23). The second condition in Eq. (26) places a lower bound on the value of the baseline damping gain. It is clear that the inequality is satisfied for any positive gain K_D^f. Finally, the third inequality follows from the previous two.

Remark 3: If the time derivative of the filtered tracking error $\dot{e}_1^f(t)$ is driven to become small then the original tracking-error signal $e_1(t)$ will also become small. This statement directly follows from the definition in Eq. (19). In fact, the latter can be written as

$$\dot{e}_1 = -k_1 e_1 + \dot{e}_1^f \tag{27}$$

whose explicit solution is

$$e_1(t) = e^{-k_1(t-t_0)}e_1(t_0) + \int_{t_0}^{t} e^{-k_1(t-\tau)}\dot{e}_1^f(\tau)\,\mathrm{d}\tau \tag{28}$$

Consequently, if there exists T such that $|\dot{e}_1^f(t)| \le \varepsilon_1$ for all $t \ge t_0 + T$, then as $t \to \infty$,

$$\begin{aligned} |e_1(t)| &\le e^{-k_1(t-t_0-T)}|e_1(t_0)| + \varepsilon_1 \int_{t_0+T}^{t} e^{-k_1(t-\tau)}\,\mathrm{d}\tau \\ &= e^{-k_1(t-t_0-T)}|e_1(t_0)| + \frac{\varepsilon_1}{k_1}(1 - e^{-k_1(t-t_0-T)}) \to \frac{\varepsilon_1}{k_1} \end{aligned} \tag{29}$$

In other words, the absolute value of the original tracking error $|e_1(t)|$ approaches $\frac{\varepsilon_1}{k_1}$, exponentially fast, and its transient dynamics depend on the time constant $\frac{1}{k_1}$.

Remark 4: If the filtered tracking error $e_1^f(t)$ is driven to become small then the original tracking-error signal $e_1(t)$ will also become small. Integrating Eq. (28) by parts yields

$$\begin{aligned} e_1(t) &= e^{-k_1(t-t_0)}e_1(t_0) + \int_{t_0}^{t} e^{-k_1(t-\tau)}\dot{e}_1^f(\tau)\,\mathrm{d}\tau = e^{-k_1(t-t_0)}e_1(t_0) \\ &+ e^{-k_1(t-\tau)}e_1^f(\tau)|_{t_0}^{t} - k_1\int_{t_0}^{t} e^{-k_1(t-\tau)}e_1^f(\tau)\,\mathrm{d}\tau = e^{-k_1(t-t_0)}(e_1(t_0) \\ &- e_1^f(t_0)) + e_1^f(t) - k_1\int_{t_0}^{t} e^{-k_1(t-\tau)}e_1^f(\tau)\,\mathrm{d}\tau \end{aligned} \tag{30}$$

Consequently, if there exists T such that $|e_1^f(t)| \le \varepsilon_1$ for all $t \ge T + t_0$, then as $t \to \infty$

$$\begin{aligned} |e_1(t)| &\le e^{-k_1(t-t_0-T)}|e_1(t_0+T) - e_1^f(t_0+T)| + \varepsilon_1 \\ &+ k_1\varepsilon_1\int_{t_0+T}^{t} e^{-k_1(t-\tau)}\,\mathrm{d}\tau \le e^{-k_1(t-t_0-T)}|e_1(t_0+T) \\ &- e_1^f(t_0+T)| + \varepsilon_1 + \varepsilon_1(1 - e^{-k_1(t-t_0-T)}) \to 2\varepsilon_1 \end{aligned} \tag{31}$$

In other words, if $|e_1^f(t)| \le \varepsilon_1$ then as $t \to \infty$ the following asymptotic relation takes place,

$$|e_1(t)| \le 2\varepsilon_1 + o(1) \tag{32}$$

where $o(1)$ denotes the small-o symbol [7].

III. Online Uncertainty Representation

This section discusses linear-in-parameters representation of the system uncertainties. The reader should immediately note that an online approximation of the uncertainty is not needed, nor it is required in the proposed design. For this very reason, the word representation is used as opposed to approximation, since the latter would require persistency of excitation conditions [8,9] that are not verifiable in real-time operation of the system.

Linear-in-parameters online representation of the uncertain function $D(\bar{x})$ in Eq. (10) is performed on a compact $\bar{x}$ region Ω, using an N–dimensional regressor vector $\Phi_D(\bar{x}) \in R^N$, with radial basis functions (RBFs) [10]:

$$\hat{D}(\bar{x}) = \hat{\theta}_D^T \Phi_D(\bar{x}) \tag{33}$$

where $\hat{\theta}_D \in R^N$ is the vector of online estimated parameters. It is assumed that the number of RBF components N is large enough, and the components are chosen so that the uncertainty $D(\bar{x})$ can be represented within the prescribed tolerance $\varepsilon_D^{\max}$, on the chosen compact $\bar{x}$ region Ω:

$$D(\bar{x}) = (\theta_D^*)^T \Phi_D(\bar{x}) + \varepsilon_D(\bar{x}) \tag{34}$$

In Eq. (34), θ_D^* denotes the vector of true unknown constant parameters, and ε_D is the unknown bounded representation error, with the known upper bound:

$$|\varepsilon_D(\bar{x})| \le \varepsilon_D^{\max} \tag{35}$$

Subtracting Eq. (34) from Eq. (33), the function representation error can be expressed in terms of the parameter estimation error:

$$e_D \triangleq \hat{D} - D = \underbrace{(\hat{\theta}_D - \theta_D^*)^T}_{\Delta\theta_D}\Phi_D - \varepsilon_D = \Delta\theta_D^T\Phi_D - \varepsilon_D \tag{36}$$

Substituting Eq. (36) into Eq. (24), the closed-loop filtered tracking-error dynamics can be derived in the form

$$\dot{e}_f = A_{\text{ref}}e_f - b_{\text{ref}}((1-\bar{\gamma})(\Delta\theta_D^T\Phi_D - \varepsilon_D) + \bar{\gamma}(v_{sl} - D) + \hat{k}_D^f\eta) \tag{37}$$

IV. Parameter Adaptation and Closed-Loop System Dynamics

Choose a symmetric positive-definite matrix $Q > 0$ and solve the following algebraic Lyapunov equation:

$$PA_{\text{ref}} + A_{\text{ref}}^T P = -Q \tag{38}$$

Since A_{ref} is Hurwitz, the Lyapunov equation has the unique positive-definite symmetric solution P, which is used to introduce a Lyapunov function candidate in the form

$$V(e_f, \Delta\theta_D) = e_f^T Pe + \Delta\theta_D\Gamma_D^{-1}\Delta\theta_D + \gamma_D^{-1}(\hat{k}_D^f)^2 \tag{39}$$

where symmetric positive-definite matrix Γ_D and positive scalar γ_D define the rates of adaptation. Differentiating Eq. (39) along the trajectories of the system (24) yields

$$\begin{aligned}\dot{V} = &-e_f^T Qe_f + 2(1-\bar{\gamma})e_f^T Pb_{\text{ref}}(-\Delta\theta_D^T\Phi_D + \varepsilon_D)\\ &- 2e_f^T Pb_{\text{ref}}\hat{k}_D^f\eta + 2\Delta\theta_D^T\Gamma_D^{-1}\dot{\hat{\theta}}_D + 2\gamma_D^{-1}\hat{k}_D^f\dot{\hat{k}}_D^f\\ &- 2\bar{\gamma}(v_{sl} - D)e_f^T Pb_{\text{ref}}\end{aligned} \tag{40}$$

Regrouping the terms, further gives

$$\begin{aligned}\dot{V} = &-e_f^T Qe_f + 2e_f^T Pb_{\text{ref}}(1-\bar{\gamma})\varepsilon_D + 2\bar{\gamma}(D - v_{sl})e_f^T Pb_{\text{ref}}\\ &+ 2\Delta\theta_D^T(-\Phi_D(1-\bar{\gamma})e_f^T Pb_{\text{ref}} + \Gamma_D^{-1}\dot{\hat{\theta}}_D) + 2\hat{k}_D^f(-e_f^T Pb_{\text{ref}}\eta\\ &+ \gamma_D^{-1}\dot{\hat{k}}_D^f)\end{aligned} \tag{41}$$

To make the time derivative $\dot{V}$ in Eq. (41) negative outside of a compact $(e, \Delta\theta_D, \hat{k}_D^f)$ subset of Ω, choose the following parameter adaptation laws:

$$\begin{aligned}\dot{\hat{\theta}}_D &= \Gamma_D\text{proj}(\hat{\theta}_D, \Phi_D\underbrace{e_f^T Pb_{\text{ref}}}_{\bar{e}_f(t)}(1-\bar{\gamma}))\\ \dot{\hat{k}}_D^f &= \gamma_D\text{proj}(\hat{k}_D^f, \eta\underbrace{e_f^T Pb_{\text{ref}}}_{\bar{e}_f(t)})\end{aligned} \tag{42}$$

In Eq. (42), proj denotes the projection operator [11], which forces the adaptive parameters to evolve in a prespecified $(\Delta\theta_D, \hat{k}_D^f)$ region. Furthermore, it is easy to see that

$$\bar{e}_f(t) \triangleq e_f^T Pb_{\text{ref}} = p_{12}e_1^f + p_{22}\dot{e}_1^f + p_{32}\eta \tag{43}$$

Motivated by the state-limiting idea from [6], the SL component of the controller is defined as

$$v_{sl} = K_{sl}\text{sat}\left(\frac{\bar{e}_f}{\varepsilon}\right) = K_{sl}\text{sat}\left(\frac{p_{12}e_1^f + p_{22}\dot{e}_1^f + p_{32}\eta}{\varepsilon}\right) \tag{44}$$

where K_{sl} is a sufficiently large positive constant gain, $0 < \varepsilon \ll 1$ is the error tolerance, and

$$\text{sat}(s) = \max(-1, \min(s, 1)) \tag{45}$$

is the saturation function. Note that in [6], the state-limiting logic uses the sign function, while this proposed design is based on the saturation function (45). The latter avoids the undesirable effects of abrupt switching and as a result, it provides continuous transition between subsystems of the proposed controller. Substituting Eqs. (42–44) into Eq. (41) yields

$$\begin{aligned}\dot{V} = &-e_f^T Qe_f + 2\bar{\gamma}\left(D - K_{sl}\text{sat}\left(\frac{\bar{e}_f(t)}{\varepsilon}\right)\right)\bar{e}_f(t)\\ &+ 2\bar{e}_f(t)(1-\bar{\gamma})\varepsilon_D\end{aligned} \tag{46}$$

Recall that the state-dependent modulation function $\bar{\gamma}(\bar{x})$ is defined as in Eq. (13).

Assumption 1: The command x_1^{cmd} for the reference model (2) is chosen such that

$$(x_1^m(t) \quad x_2^m(t) \quad z(t) \quad \dot{z}(t))^T \in \Omega_\delta \tag{47}$$

forward in time. Next, one must show closed-loop stability and boundedness of the error dynamics.

Suppose that $|\bar{e}_f(t)| > \varepsilon$. Then,

$$\text{sat}\left(\frac{\bar{e}_f(t)}{\varepsilon}\right) = \text{sgn}(\bar{e}_f(t)) \tag{48}$$

To analyze closed-loop stability, consider three distinct cases.

In case 1, if $\bar{x} \notin \Omega$, then $\bar{\gamma} = 1$ and choosing

$$K_{sl} \geq D_{\max} \tag{49}$$

relation (46) becomes

$$\begin{aligned}\dot{V} &= -e_f^T Qe_f + 2(D - K_{sl}\text{sgn}\bar{e}_f(t))\bar{e}_f(t) = -e_f^T Qe_f\\ &+ 2(D\text{sgn}\bar{e}_f(t) - K_{sl})|e_f(t)| \leq -\lambda_{\min}(Q)\|e_f(t)\|^2\\ &+ 2\underbrace{(D_{\max} - K_{sl})}_{<0}|e_f^T Pb_{\text{ref}}| \leq -\lambda_{\min}(Q)\|e_f\|^2\end{aligned} \tag{50}$$

Consequently, the tracking error will decay until the system state enters Ω.

In case 2, if $\bar{x} \in \Omega_\delta$ then according to Eq. (13) $\bar{\gamma} = 0$, and therefore

$$\begin{aligned}\dot{V} = -e_f^T Qe_f + 2e_f^T Pb_{\text{ref}}\varepsilon_D \leq -\lambda_{\min}(Q)\|e_f\|^2\\ + 2\|e_f\|\|Pb_{\text{ref}}\|\varepsilon_D^{\max}\end{aligned} \tag{51}$$

where $\lambda_{\min}(Q)$ is the minimum eigenvalue of Q, $\varepsilon_D^{\max} \triangleq \max_{\bar{x}\in\Omega}\varepsilon_D(\bar{x})$. Also note that because of the projection operator, norms of the parameter estimation errors will stay uniformly bounded; that is,

$$\|\Delta\theta(t)\| \leq \Delta\theta_{\max} < \infty \wedge \|\hat{k}_D^f(t)\| \leq (\hat{k}_D^f)_{\max} < \infty \tag{52}$$

where $[\Delta\theta_{\max}, (\hat{k}_D^f)_{\max}]$ are the parameter bounds.

Using Eq. (51), uniform ultimate boundedness (UUB) [12] of the closed-loop system trajectories can now be established. Toward that end, define the following compact subset in the e_f region:

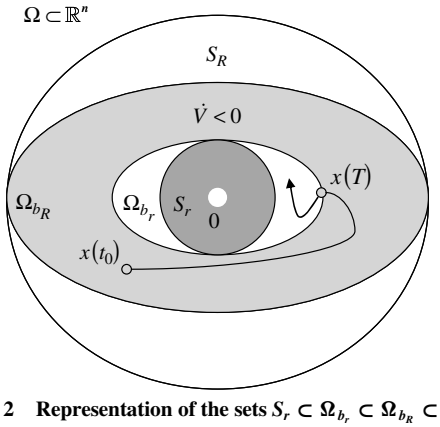

Fig. 2 Representation of the sets $S_r \subset \Omega_{b_r} \subset \Omega_{b_R} \subset S_R$.

$$S_r \triangleq \left\{ \|e_f\| \le r \triangleq \frac{2\|Pb_{\text{ref}}\|\varepsilon_D^{\max}}{\lambda_{\min}(Q)} \right\} \tag{53}$$

Also define a minimal level set $\Omega_{b_r} = \{e_f^T P e_f \le b_r\}$ that contains S_r. Since

$$\lambda_{\min}(P)\|e_f\|^2 \le e_f^T P e_f \le \lambda_{\max}(P)\|e_f\|^2 \tag{54}$$

then choosing

$$b_r = \lambda_{\max}(P) r^2 \tag{55}$$

implies that for all $\|e_f\| \le r$

$$e_f^T P e_f \le \lambda_{\max}(P)\|e_f\|^2 \le \lambda_{\max}(P) r^2 = b_r \tag{56}$$

Hence, the set S_r is contained in the level set Ω_{b_r}.

Suppose that all *initial* values of the filtered tracking error $e_f(t_0)$ belong to a compact set $S_R \triangleq \{\|e_f\| \le R\}$. Let $\Omega_{b_R} = \{e_f^T P e_f \le b_R\}$ be the maximal level set which belongs to S_R. To maintain closed-loop system stability, a specific relation between the boundaries for the sets Ω_{b_r}, Ω_{b_R}, S_r, and S_R must be imposed. These sets will be used to prove that the closed-loop system trajectories are UUB. Graphical representation of the four sets is given in Fig. 2.

Choose:

$$b_R = \lambda_{\min}(P) R^2 \tag{57}$$

Then if $e_f^T P e_f \le B$ then using Eq. (54) yields

$$\lambda_{\min}(P)\|e_f\|^2 \le e_f^T P e_f \le B = \lambda_{\min}(P) R^2 \tag{58}$$

Consequently, $\|e_f\| \le R$; that is, the filtered tracking error is in S_R. Because of Eqs. (51) and (53), the time derivative $\dot{V}$ is negative outside of S_r. Therefore, the filtered tracking error e_f will enter level set Ω_{b_r} in finite time, and will remain in the set from then on. So, the closed-loop system trajectories are UUB.

In case 3, if $\bar{x} \in \Omega - \Omega_\delta$ then both the adaptive and the SL components of the controller are active. In this case, using Eq. (46) one gets

$$\begin{aligned} \dot{V} &= -e_f^T Q e_f + 2\bar{\gamma}(D - K_{sl}\text{sgn}(\bar{e}_f(t))\bar{e}_f(t) + 2\bar{e}_f(t)(1-\bar{\gamma})\varepsilon_D) \\ &\le -\lambda_{\min}(Q)\|e_f\|^2 + 2[\bar{\gamma}(D_{\max} - K_{sl}) + (1-\bar{\gamma})\varepsilon_D^{\max}]|e_f^T P b_{\text{ref}}| \\ &\le -\lambda_{\min}(Q)\|e_f\|^2 + 2(1-\bar{\gamma})\|e_f\|\|Pb_{\text{ref}}\|\varepsilon_D^{\max} \end{aligned} \tag{59}$$

Since by definition $0 \le \bar{\gamma} \le 1$,

$$\begin{aligned} \dot{V} &\le -\lambda_{\min}(Q)\|e_f\|^2 + 2(1-\bar{\gamma})\|e_f\|\|Pb_{\text{ref}}\|\varepsilon_D^{\max} \\ &\le -\lambda_{\min}(Q)\|e_f\|^2 + 2\|e_f\|\|Pb_{\text{ref}}\|\varepsilon_D^{\max} \end{aligned} \tag{60}$$

Similar to case 2, one can show that the system trajectories will enter the sub region Ω_δ in finite time, after which the case 2 conditions take place.

These three cases prove the UUB property of the closed-loop system trajectories provided that the relation (48) takes place. If it does not [that is, if $|\bar{e}_f(t)| \le \varepsilon$], then it is sufficient to choose $\varepsilon = r$, with r defined as in Eq. (53). Then, because of Eq. (56), the corresponding trajectory must be in Ω_{b_r}, and it will evolve inside the compact forward in time. Moreover, due to the use of the projection operator in Eq. (42), all the estimated parameters $\hat{\theta}(t)$ are bounded. Hence, the tracking problem is solved.

In summary, the corresponding total explicit model following control signal can be written using Eqs. (7), (12), (22), (33), and (44):

$$\begin{aligned} \dot{x}_2^{\text{cmd}} = &\underbrace{B_1^{-1}\left(\ddot{x}_1^m - f(\bar{x}) - K_D(\dot{\hat{x}}_1 - \dot{x}_1^m) - K_P(x_1 - x_1^m) - K_I\left(\frac{x_1(t) - x_1^m(t)}{s}\right)\right)}_{\text{baseline dynamic Inversion controller}} - (1-\bar{\gamma}(\bar{x}))\underbrace{B_1^{-1}\hat{\theta}_D^T(t)\Phi_D(\bar{x})}_{\text{adaptive augmentation}} \\ - &\underbrace{\bar{\gamma}(\bar{x})}_{\text{modulation function}}\underbrace{B_1^{-1}K_{sc}\text{sat}\left(\frac{p_{12}e_1^f + p_{22}\dot{e}_1^f + p_{23}\eta}{\varepsilon}\right)}_{\text{state limiter}} - \underbrace{B_1^{-1}(K_D^f + \hat{k}_D^f)\eta}_{\text{additional Rate damping}} \end{aligned} \tag{61}$$

Remark 5: Via Eq. (21), the damping term in Eq. (22) can be written as

$$\begin{aligned} w = (K_D^f + \hat{k}_D^f)\left(\frac{sa}{s+a}\right)\underbrace{\frac{(s+k_1)}{s}(x_1 - x_1^m)}_{e_1^f} = (K_D^f \\ + \hat{k}_D^f)k_1\underbrace{\frac{((s/k_1)+1)}{((1/a)s+1)}}_{G(s)=\text{lead-lag filter}}(x_1 - x_1^m) \end{aligned} \tag{62}$$

Using Eq. (62) and separating the damping terms, allows the total control to be reformulated as

$$\begin{aligned} \dot{x}_2^{\text{cmd}} = &\underbrace{B_1^{-1}\left(\ddot{x}_1^m - f(\bar{x}) - \left(\overbrace{K_D s + K_P + \frac{K_I}{s}}^{\text{PID controller}} + K_D^f \overbrace{G(s)}^{\text{lead lag}}\right)(x_1 - x_1^m)\right)}_{\text{baseline dynamic inversion controller}} - (1-\bar{\gamma}(\bar{x}))\underbrace{B_1^{-1}\hat{\theta}_D^T(t)\Phi_D(\bar{x})}_{\text{adaptive augmentation}} \\ - &\underbrace{\bar{\gamma}(\bar{x})}_{\text{modulation function}}\underbrace{B_1^{-1}K_{sc}\text{sat}\left(\frac{p_{12}e_1^f + p_{22}\dot{e}_1^f + p_{23}\eta}{\varepsilon}\right)}_{\text{state limiter}} - \underbrace{B_1^{-1}\hat{k}_D^f G(s)(x_1 - x_1^m)}_{\text{adaptive rate damping}} \end{aligned} \tag{63}$$

From Eq. (63), it follows that the total control signal is composed of the following five major components: 1) baseline dynamic inversion controller, 2) adaptive augmentation, 3) state limiter, 4) modulation function, and 5) adaptive rate damping.

The control architecture (63) was developed for a class of second-order systems in the cascaded form [Eq. (1)]. This particular class of systems was chosen primarily to clarify and expose key features of the design process. These systems also naturally appear in flight dynamics and control problems, which constitute the primary focus and motivation for the control development. One may immediately note that since the design is based on the dynamic inversion method, the developed controller can be extended to a generic class of feedback linearizable MIMO systems with cascade-connected dynamics.

Remark 6: As discussed in the Introduction, the modulation function $\bar{\gamma}(\bar{x})$ in Eq. (63) enforces prespecified bounds for the closed-loop system trajectories. In flight control applications, such a component is often called the state limiter. In practice, all realistic flight control devices are equipped with state limiters of various forms. The particular state limiter presented in this paper is novel. Recently, it was implemented and flight verified on the Boeing/NASA X-48B blended-wing-body (BWB) experimental aircraft. BWB state limiter design and flight test evaluation results will be reported in the near future.

V. Design Example: AOA Tracking for a Generic Aerial Vehicle

This section applies the developed adaptive control methodology to construct an AOA tracking system for a fixed-wing aircraft, whose short-period dynamics, including lift and pitching-moment uncertainties, can be written in the form of Eq. (1) [1,4]:

$$\begin{cases} \dot{\alpha} = -\tilde{L}_\alpha \alpha + Q_{\text{grav}} + q + \Delta L(\alpha) \\ \dot{q} = M(\alpha) + M_q q + M_{IC} + \dot{q}_{\text{cmd}} + \Delta M(\alpha, q) \end{cases} \tag{64}$$

where α is aircraft AOA, q is the angular pitch rate, $\tilde{L}_\alpha$ is the known lift-curve slope, Q_{grav} is the known gravity term, $\Delta L(\alpha)$ is the lift force uncertainty, $M(\alpha)$ is the known static stability (pitching moment), M_q is the known constant pitch damping, M_{IC} is the known pitching-moment increment due to inertial cross-coupling effects, and $\dot{q}_{\text{cmd}}$ is the commanded pitch acceleration (control input), and $\Delta M(\alpha, q)$ represents the pitching-moment uncertainty.

The AOA desired/reference model dynamics is chosen in the form of Eq. (2):

$$\alpha_m = \left[\frac{\omega^2}{s^2 + 2\xi\omega s + \omega^2}\right]\alpha_{\text{cmd}} \Leftrightarrow \ddot{\alpha}_m = -2\xi\omega\dot{\alpha}_m + \omega^2(\alpha_{\text{cmd}} - \alpha_m) \tag{65}$$

Following Eq. (62), the rate damping term is chosen as

$$w = \frac{(K_D^f + \hat{k}_D^f)}{(\frac{s}{a} + 1)}(q - q_m) = \underbrace{K_D^f \frac{a}{(s+a)}(q - q_m)}_{\text{Baseline}} + \underbrace{\hat{k}_D^f(t)\frac{a}{(s+a)}(q - q_m)}_{\text{Adaptive}} \tag{66}$$

The baseline dynamic inversion controller $\dot{q}_{\text{cmd}}^{bl}$ with the baseline rate damping term included can now be written as,

$$\dot{q}_{\text{cmd}}^{bl} = \dot{q}_m - M_\alpha \alpha - M_q q - M_{\text{IC}} - \left[2\xi\omega + K_D^f \frac{a}{s+a}\right](q - q_m) - \omega^2 \frac{(q - q_m)}{s} \tag{67}$$

where

$$q_m \triangleq \dot{\alpha}_m + \tilde{L}_\alpha \alpha_m - Q_{\text{grav}} \tag{68}$$

is the reference model pitch rate signal. The pitch rate error can be written in terms of the AOA tracking error as

$$q_m - q = (s + \tilde{L}_\alpha)(\alpha_m - \alpha) \tag{69}$$

To perform the design, one needs to match the required components against the corresponding AOA/pitch rate dynamics terms. Comparing Eq. (64) against the generic cascaded dynamics (1) yields

$$\begin{gathered} x_1 = \alpha, \quad x_2 = q, \quad z = (Q_{\text{grav}} \;\; M_{\text{IC}})^T, \quad \dot{x}_2^{\text{cmd}} = \dot{q}_{\text{cmd}} \\ F_1 = -\tilde{L}_\alpha \alpha + Q_{\text{grav}}, \quad B_1 = 1, \quad F_2 = M(\alpha) + M_q q + M_{\text{IC}} \\ f_1 = \Delta L(\alpha), \quad f_2 = \Delta M(\alpha, q) \end{gathered} \tag{70}$$

In this case, the baseline PID feedback gains are

$$\begin{gathered} K_{\dot{\alpha}} \triangleq K_D = 2\xi\omega + k_1 \qquad K_\alpha \triangleq K_P = \omega(\omega + 2\xi k_1) \\ K_\alpha^I \triangleq K_I = \omega^2 k_1 \end{gathered} \tag{71}$$

where the integrator pole k_1 is chosen as

$$k_1 = \tilde{L}_\alpha \tag{72}$$

Using Eq. (19), the filtered tracking-error signal becomes

$$e_1^f = \frac{(s + k_1)}{s} e_1 = \frac{(s + \tilde{L}_\alpha)}{s}(\alpha_m - \alpha) = \frac{q_m - q}{s} \tag{73}$$

Hence, the filtered tracking vector is

$$e_f = \begin{pmatrix} e_1^f & \dot{e}_1^f & \frac{a}{(s+a)}\dot{e}_1^f \end{pmatrix}^T = \begin{pmatrix} \frac{q_m - q}{s} & q_m - q & \frac{a}{(s+a)}(q_m - q) \end{pmatrix}^T \tag{74}$$

The regressor vector Φ_D is chosen to depend on AOA only. Then parameter adaptation laws are written based on Eq. (42):

$$\begin{aligned} \dot{\hat{\theta}}_D &= \Gamma_D \text{proj}\left(\hat{\theta}_D, \Phi_D(\alpha)\begin{pmatrix} \frac{q_m - q}{s} & q_m - q & \frac{a}{(s+a)}(q_m - q) \end{pmatrix} \right. \\ &\left. \times P\begin{pmatrix} 0 \\ 1 \\ 0 \end{pmatrix}(1 - \bar{\gamma})\right) \\ \dot{\hat{k}}_D^f &= \gamma_D \text{proj}\left(\hat{k}_D^f, \eta\begin{pmatrix} \frac{q_m - q}{s} & q_m - q & \frac{a}{(s+a)}(q_m - q) \end{pmatrix} P\begin{pmatrix} 0 \\ 1 \\ 0 \end{pmatrix}\right) \end{aligned} \tag{75}$$

where $P = P^T > 0$ is the unique positive-definite symmetric solution of the algebraic Lyapunov equation (38) with the Hurwitz reference model matrix A_{ref} as specified in Eq. (24).

Based on Eq. (33), adaptive pitch acceleration command takes the form

$$\dot{q}_{\text{cmd}}^{\text{ad}} = \hat{\theta}_D^T(t)\Phi_D(\alpha) \tag{76}$$

Using Eq. (44), the SL component of the pitch acceleration command becomes

$$\dot{q}_{\text{cmd}}^{\text{sl}} = K_{\text{sl}} \text{sat}\left(\frac{\bar{e}_f}{\varepsilon}\right) = K_{\text{sl}} \text{sat}\left(\frac{p_{12}e_1^f + p_{22}\dot{e}_1^f + p_{32}\eta}{\varepsilon}\right)\alpha \tag{77}$$

Relation (66) defines adaptive rate damping component of the pitch acceleration command:

$$\dot{q}_{\text{cmd}}^{\text{ad}_D} = \hat{k}_D^f(t)\frac{a}{(s+a)}(q_m - q) \tag{78}$$

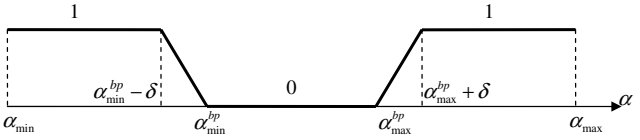

Fig. 3 Piecewise linear modulation function.

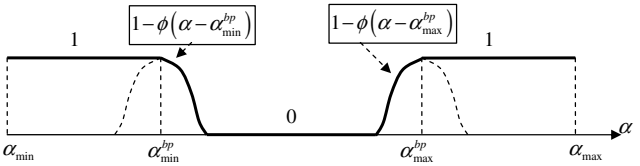

Fig. 4 RBF-based smooth modulation function.

To provide an example of the modulation function first introduced in Eq. (13), let $\Omega = (\alpha_{\min}^{bp} \quad \alpha_{\max}^{bp})$ denote the AOA allowable domain, where $\alpha_{\min}^{bp} \geq \alpha_{\min}$ and $\alpha_{\max}^{bp} \leq \alpha_{\max}$ are the AOA minimum and maximum break points, correspondingly. Piecewise linear modulation function $\bar{\gamma}(\alpha)$ can be easily written to satisfy Eq. (13):

$$\bar{\gamma}(\alpha) = \begin{cases} 1, & \alpha \leq \alpha_{\min}^{bp} - \delta \\ \frac{\alpha_{\min}^{bp} - \alpha}{\delta}, & \alpha_{\min}^{bp} - \delta < \alpha \leq \alpha_{\min}^{bp} \\ 0, & \alpha_{\min}^{bp} < \alpha < \alpha_{\max}^{bp} \\ \frac{\alpha - \alpha_{\max}^{bp}}{\delta}, & \alpha_{\max}^{bp} \leq \alpha < \alpha_{\max}^{bp} + \delta \\ 1, & \alpha \geq \alpha_{\max}^{bp} + \delta \end{cases} \tag{79}$$

Figure 3 shows a sketch of the modulation function.

If desired, a *smooth* version of the modulation function can be created using two endpoint RBFs.

$$\bar{\gamma}(\alpha) = \begin{cases} 1 - \phi(\alpha - \alpha_{\min}^{bp}), & \alpha \leq \alpha_{\min}^{bp} \\ 0, & \alpha_{\min}^{bp} < \alpha < \alpha_{\max}^{bp} \\ 1 - \phi(\alpha - \alpha_{\max}^{bp}), & \alpha \geq \alpha_{\max}^{bp} \end{cases} \tag{80}$$

This function is shown in Fig. 4.

In the above, δ represents the break point increment, which is used to place RBFs uniformly on the interval $(\alpha_{\min}^{bp} \quad \alpha_{\max}^{bp})$.

A multidimensional modulation function $\bar{\gamma}(\bar{x})$ can also be formed as follows. Suppose that $\bar{x}_0$ is the center point of the sphere $\Omega_R = \{\|\bar{x} - \bar{x}_0\| \leq R\}$. Also suppose that the set Ω_R represents the allowable state domain. Let $\delta > 0$ be a small positive constant and define $\Omega_{R-\delta} = \{\|\bar{x} - \bar{x}_0\| \leq R - \delta\}$. The multidimensional modulation function is defined as

$$\bar{\gamma}(\bar{x}) = \begin{cases} 0, & \bar{x} \in \Omega_{R-\delta} \\ 0 \leq \bar{\gamma}(\bar{x}) \leq 1, & \bar{x} \in \Omega_R - \Omega_{R-\delta} \\ 1, & \bar{x} \notin \Omega_R \end{cases} \tag{81}$$

Formally, the modulation function can be written as

$$\bar{\gamma}(x) = \max\left[0, \min\left[1, 1 + \frac{\|\bar{x} - \bar{x}_0\| - R}{\delta}\right]\right] \tag{82}$$

To see that Eq. (82) implies Eq. (81) it is sufficient to simply sketch $\bar{\gamma}(\bar{x})$ versus $\|\bar{x} - \bar{x}_0\|$. Figure 5 shows the data.

Using Eq. (82) yields three relations that formally prove the validity of the modulation function:

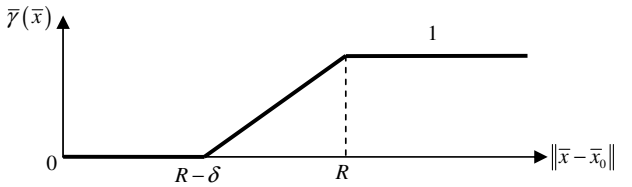

Fig. 5 Multidimensional modulation function.

$$\bar{\gamma}(\bar{x}) = 0 \Leftrightarrow 1 + \frac{\|\bar{x} - \bar{x}_0\| - R}{\delta} \leq 0 \Leftrightarrow \|\bar{x} - \bar{x}_0\| \leq R - \delta \Leftrightarrow \bar{x} \in \Omega_{R-\delta}$$

$$\bar{\gamma}(\bar{x}) = 1 \Leftrightarrow 1 + \frac{\|\bar{x} - \bar{x}_0\| - R}{\delta} \geq 1 \Leftrightarrow \|\bar{x} - \bar{x}_0\| \geq R \Leftrightarrow \bar{x} \notin \Omega_R$$

$$0 \leq \bar{\gamma}(\bar{x}) \leq 1 \Leftrightarrow 0 \leq 1 + \frac{\|\bar{x} - \bar{x}_0\| - R}{\delta} \leq 1 \Leftrightarrow R - \delta \leq \|\bar{x} - \bar{x}_0\| \leq R \Leftrightarrow \bar{x} \in \Omega_{R-\delta}$$

For example, suppose that $\bar{x} = (\alpha \quad \dot{\alpha})$ and $\bar{x}_0 = (\alpha_0 \quad 0)$. Choose the L_1-weighted norm with the weights set to $1/\alpha_{\max}$ and $1/\dot{\alpha}_{\max}$. Choosing $R = 1$, $\delta = 0.1$ yields the corresponding two-dimensional modulation function:

$$\bar{\gamma}(\alpha, \dot{\alpha}) = \max\left[0, \min\left[1, 1 + \frac{\frac{|\alpha - \alpha_0|}{\alpha_{\max}} + \frac{|\dot{\alpha}|}{\dot{\alpha}_{\max}} - 1}{0.1}\right]\right]$$

In this case,

$$\Omega_1 = \left\{\frac{|\alpha - \alpha_0|}{\alpha_{\max}} + \frac{|\dot{\alpha}|}{\dot{\alpha}_{\max}} \leq 1\right\}$$

$$\Omega_{0.9} = \left\{\frac{|\alpha - \alpha_0|}{\alpha_{\max}} + \frac{|\dot{\alpha}|}{\dot{\alpha}_{\max}} \leq 0.9\right\}$$

Consequently, the modulation function is

$$\bar{\gamma}(\alpha, \dot{\alpha}) = \begin{cases} 0, & |\alpha - \alpha_0| \leq 0.9\alpha_{\max} \wedge |\dot{\alpha}| \leq 0.9\dot{\alpha}_{\max} \\ 1, & |\alpha - \alpha_0| > \alpha_{\max} \vee |\dot{\alpha}| > \dot{\alpha}_{\max} \end{cases}$$

Otherwise, it takes values between 0 and 1.

In summary, total pitch acceleration command consists of the five terms: 1) baseline dynamic inversion command (67), 2) adaptive augmentation (76), 3) state limiter (77), 4) AOA modulation function $\bar{\gamma}(\alpha)$, and 5) adaptive rate damping component (78):

$$\dot{q}_{\text{cmd}} = \dot{q}_{cmd}^{\text{bl}} + (1 - \bar{\gamma}(\alpha))\dot{q}_{\text{cmd}}^{\text{ad}} + \bar{\gamma}(\alpha)\dot{q}_{\text{cmd}}^{\text{sl}} + \dot{q}_{\text{cmd}}^{\text{ad}_D} \tag{83}$$

The simulation model is chosen to represent longitudinal dynamics of an aerial vehicle, such as an F-16 aircraft. Neglecting the effects of gravity and thrust, aircraft longitudinal (short-period) dynamics can be written in matrix form [4],

$$\underbrace{\begin{pmatrix} \dot{\alpha} \\ \dot{q} \end{pmatrix}}_{\dot{x}_p} = \underbrace{\begin{pmatrix} \frac{Z_\alpha}{V} & 1 \\ M_\alpha & M_q \end{pmatrix}}_{A_{p\text{BL}}} \underbrace{\begin{pmatrix} \alpha \\ q \end{pmatrix}}_{x_p} + \underbrace{\begin{pmatrix} \frac{Z_{\delta}}{V} \\ M_{\delta_e} \end{pmatrix}}_{B_p} \underbrace{\delta}_{\substack{e \\ u}} \tag{84}$$

where α is the aircraft AOA, q is the pitch rate, δ_e is the elevator deflection (control input), V is the trimmed (constant) airspeed, $(Z_\alpha, Z_q, Z_{\delta_e})$ and $(M_\alpha, M_q, M_{\delta_e})$ are partial derivatives of the aerodynamic vertical force Z and the pitching moment M, with respect to (α, q, δ_e), respectively. Numerical values for the vehicle aerodynamic derivatives were taken from [4] (Example 5.5-3, Table 3.4-3). These data represent an F-16 aircraft trimmed at

$$V_T = 502 \text{ ft/s}, \qquad \text{alt} = 0 \text{ ft}, \qquad \bar{Q} = 300 \text{ lb/ft}^2$$

$$\text{c.g.} = 0.35\bar{c}, \qquad \alpha = 2.11 \text{ deg}$$

The resulting open-loop system matrices are

$$A_{p\text{BL}} = \begin{pmatrix} -1.0189 & 1 \\ 0.8223 & -1.0774 \end{pmatrix}, \qquad B_p = \begin{pmatrix} -0.0022 \\ -0.1756 \end{pmatrix} \tag{85}$$

where α is in radians, q is in radians/second, and δ_e is in degrees.

Including system pitching-moment uncertainty yields updated dynamics:

$$\begin{pmatrix}\dot{\alpha}\\ \dot{q}\end{pmatrix}=\begin{pmatrix}-1.0189 & 1\\ 0.8223 & -1.0774\end{pmatrix}\begin{pmatrix}\alpha\\ q\end{pmatrix}+\begin{pmatrix}0\\ 1\end{pmatrix}\dot{q}_{\text{cmd}}+\begin{pmatrix}0\\ \Delta M(\alpha,q)\end{pmatrix} \tag{86}$$

Three types of matched uncertainties are added to the system: 1) linear-in-state uncertainty $K^T_{x_p\text{pert}}x_p$, 2) control effectiveness constant uncertainty $\Lambda > 0$, and 3) nonlinear-in-state uncertainty in the form of Eq. (34). Addition of the uncertainties updates system dynamics (86) as

$$\begin{pmatrix}\dot{\alpha}\\ \dot{q}\end{pmatrix}=\begin{pmatrix}-1.0189 & 1\\ 0.8223 & -1.0774\end{pmatrix}\begin{pmatrix}\alpha\\ q\end{pmatrix}+\begin{pmatrix}0\\ 1\end{pmatrix}\Lambda\dot{q}_{\text{cmd}}+\begin{pmatrix}0\\ K^T_{x_p\text{pert}}x_p+D(\bar{x})\end{pmatrix} \tag{87}$$

Numerical values for the uncertainties were arbitrarily chosen as

$$K^T_{x_p\text{pert}}=(\,0.4111\quad 0.8619\,),\qquad \Lambda=0.5$$
$$d(x_p)=d(\alpha)=0.5e^{-\frac{(\alpha-\alpha_c)^2}{2\sigma^2}} \tag{88}$$

where the center of the Gaussian was set to $\alpha_c = 2^\circ\pi/180$, and its width was $\sigma = 0.0233$. This particular selection of numerical values for $K^T_{x_p\text{pert}}x_p$ and Λ is equivalent to 50% increase in the static instability M_α, 80% decrease in the pitch damping M_q, and 50% decrease in the control input effectiveness. These changes imply that the vehicle became 50% more statically unstable, lost 80% of its pitch damping ability, and the aircraft controllability decreased by 50%, and in fact causes the open-loop system to become unstable (eigenvalues enter right-half-plane). Such drastic and perhaps unrealistic changes were motivated by intent to demonstrate the effectiveness of the proposed design methodology. This particular example was also selected to be similar to previous work presented in [13,14], so that relevant performance comparisons may be available. The system total uncertainty versus AOA was calculated at $q = 0$ and is shown in Fig. 6.

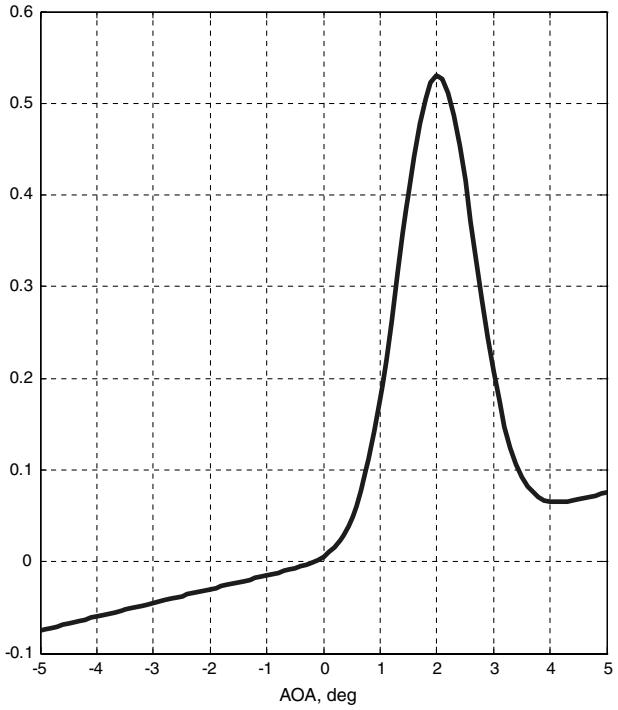

Fig. 6 Total matched uncertainty versus AOA, at $q = 0$.

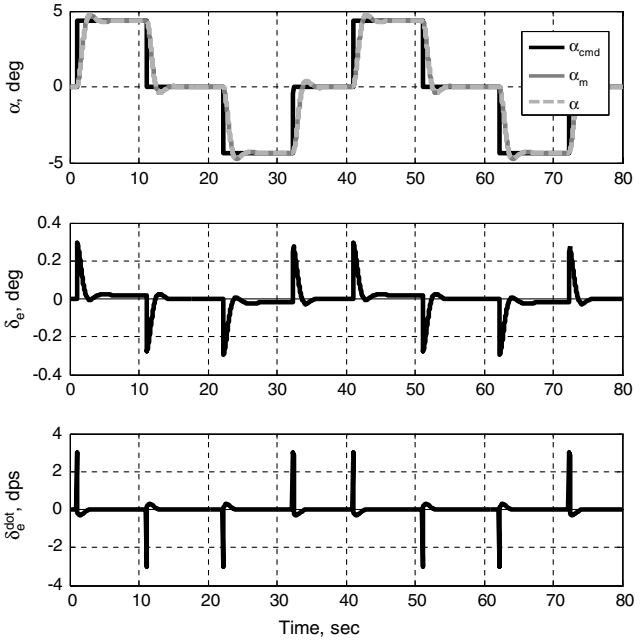

Fig. 7 Baseline closed-loop response to AOA doublets without uncertainties.

Baseline flight control was designed for the baseline system without uncertainties according to Eq. (67), with selected dynamics $\xi = 0.6$ and $\omega = 2$ rad/s, along with baseline damping gain $K^f_D = 0.1$ and desired crossover frequency $a = 10$ rad/s. It is straightforward to verify that such selections provide error dynamics roots per Eq. (25). The eigenvalues of the reference dynamics, along with their corresponding natural frequencies and damping ratios, are shown below:

$$\begin{cases}\lambda_1=-1.26+0.699i\\ \lambda_2=-1.26-0.699i\\ \lambda_3=-9.87\end{cases}\Rightarrow\begin{cases}\zeta_1=0.628, & \omega_1=2.01\\ \zeta_2=0.628, & \omega_2=2.01\\ \zeta_3=1.00, & \omega_3=9.87\end{cases} \tag{89}$$

Inspection of the eigenvalues shows that, per design, addition of the baseline damping gain K^f_D yields the reference dynamics

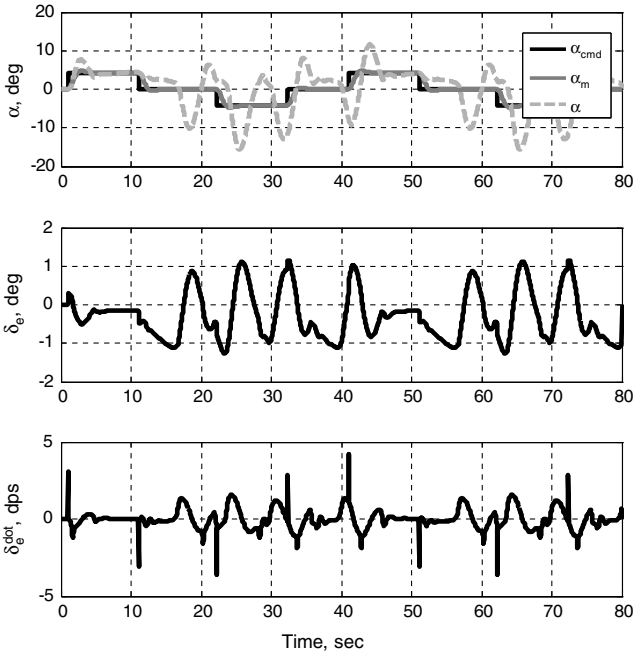

Fig. 8 Baseline closed-loop response in the presence of matched uncertainties.

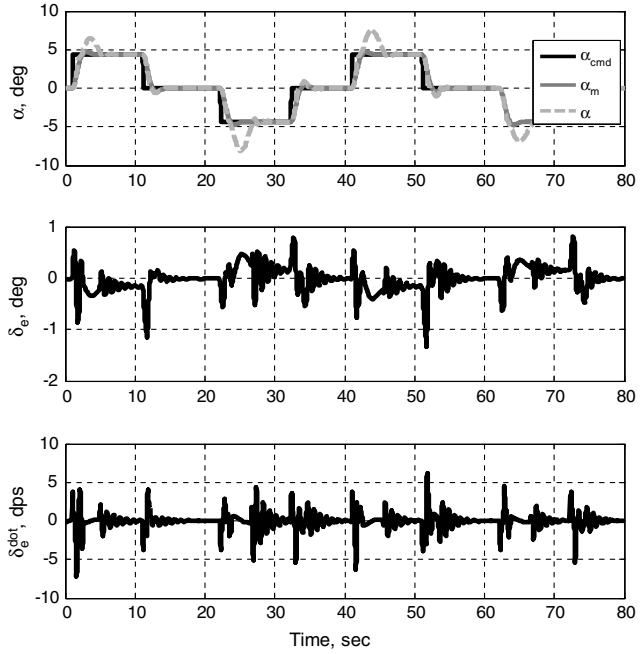

Fig. 9 Baseline plus adaptive closed-loop response in the presence of uncertainties.

containing slightly more damping than traditional dynamic inversion design. Figure 7 shows the baseline system response to a series of angle-of-attack doublets, along with the elevator deflection and rate required by the baseline controller, while tracking the AOA doublets without system uncertainties. As seen from the figure, the elevator deflection and rate are well within acceptable limits. In this simulation example, the AOA limits are set to ± 5 deg. It is important to note that the defined reference model dynamics for this example satisfy Assumption 1.

With only the baseline controller in operation and with uncertainties included, closed-loop system tracking performance degradation can be clearly observed from the data that are shown in Fig. 8. However, both the control input and its rate remain small.

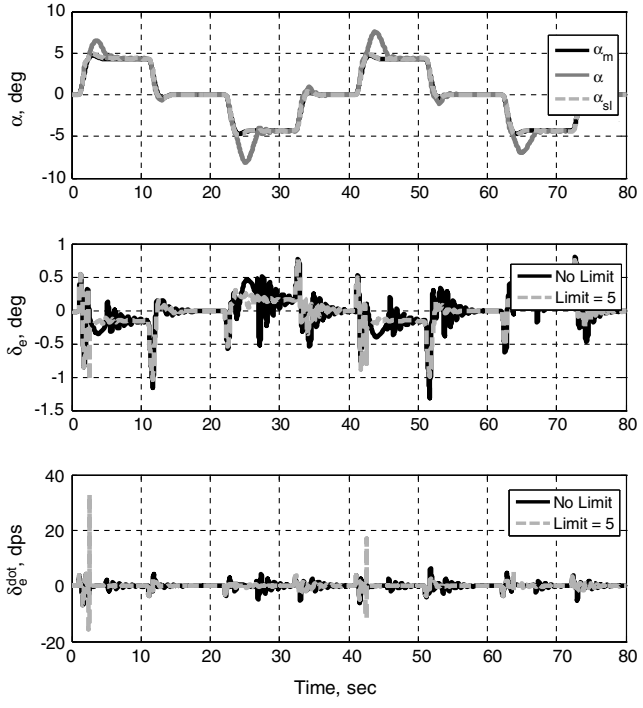

Fig. 10 Baseline plus adaptive plus SL closed-loop response in the presence of uncertainties.

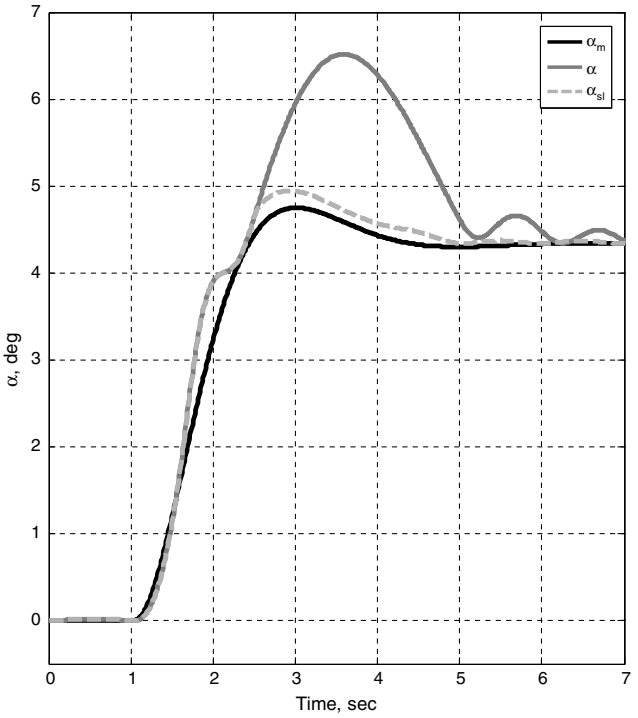

Fig. 11 Baseline plus adaptive plus SL closed-loop response in the presence of uncertainties (zoom).

Next, adaptive laws (75) were constructed by solving algebraic Lyapunov equation (38) with reference matrix A_{ref} as shown in (24). The regressor vector $\Phi_d(\alpha)$ consisted of 11 α-dependent and evenly spaced Gaussians (RBFs). RBF centers were placed at $[-10{:}2{:}10]$ degrees of AOA, and all RBF widths were set to $\sigma = 0.0233$. Rates of adaptation were chosen as

$$\Gamma_D = 100, \qquad \gamma_D = 50 \tag{90}$$

and the total control (elevator deflection) was formed as shown in Eq. (83). To show the efficacy of the adaptive augmentation without the SL component, the latter was turned off ($K_{sl} = 0$). With the (baseline plus adaptive) control components active, closed-loop

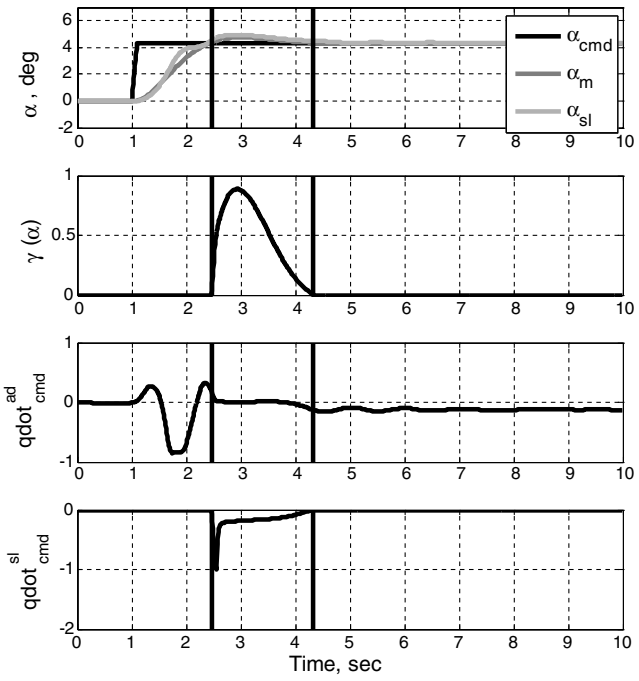

Fig. 12 Control input components (zoom).

system tracking performance was recovered, with acceptable elevator deflection and rates. The data are shown in Fig. 9.

Note that although the (baseline plus adaptive) architecture is able to restore tracking, the system AOA state constraints are violated. To show the effectiveness of the state limiter, consider simulation of the same input case but with the SL component active. Because of relationship (77) the state limiter is designed to prevent undesirable overshoots, while maintaining the benefits of the adaptive augmentation in restoring tracking response in the presence of uncertainties. Selecting $\delta = 0.1$, $K_{sc} = 2$, and $\varepsilon = 0.01$, the time response comparison of the (baseline plus adaptive plus SL) system against the (baseline plus adaptive) system without state limiting is shown in Fig. 10. In the simulation data below, the line denoted as α represents the time response of the system in the presence of uncertainties without SL component, while the line denoted as α_{sl} corresponds to the system with the SL component turned on.

A close-up view of the system response around the limit is shown in Fig. 11. The data in Fig. 11 show that the SL component is able to prevent overshoots when the system approaches state limits, while retaining the ability to restore tracking performance in the presence of uncertainties. The system response with (baseline plus adaptive) components is identical with and without the state limiter until the response is within δ of the AOA limit. With AOA limit of 5 deg and $\delta = 0.1$, the reference model AOA reaches 4.5 deg. At the same time, the system AOA tracks the reference AOA without violating the imposed AOA limit. The less oscillatory system response is also a consequence of the modulation function in the total control (83), adding damping in regions near the AOA limits.

To further clarify the role of the modulation function in the proposed state limiter logic, consider Fig. 12. These data represent the case with the (baseline plus adaptive plus SL) components turned on. The dark vertical bars indicate the region in which the modulation function is active, as shown in the second subplot. The third subplot displays the adaptive augmentation component, while the lowermost subplot displays the SL component, both including scaling as indicated in Eq. (83). When the modulation function is active, the SL component becomes also active in order to damp the system response and to avoid exceeding the AOA limit, while the adaptive augmentation component is reduced until the system leaves the state limit region.

The data from Fig. 10 indicate an increase in control activity when compared to the previous simulation cases. This is due to the presence of the adaptive damping term. One may immediately note that the proposed design gives the ability to further minimize control input activity, while enforcing the desired tracking performance. This can be accomplished by tuning the adaptive gains, SL gain, modulation function activation region, and error tolerance.

VI. Conclusions

Motivated by flight control applications, this paper presented robust adaptive control design augmentation of a baseline dynamic inversion controller. To help protect the system trajectories from leaving an allowable subset in the system state space, a state-limiting component was added to modify the control input in areas near the state limits. A frequency-dependent adaptive damping term was also incorporated into the system. The proposed design was applied to construct a representative angle-of-attack command-tracking system for short-period dynamics of a fixed-wing aircraft. Simulation results verify that the adaptive augmentation is able to restore tracking performance in the presence of significant system uncertainties, while the state-limiting component is able to modify the control input to prevent system overshooting the predefined state limits.

Acknowledgments

This work was sponsored (in part) by NASA grant number NNL06AA04B. The views and conclusions contained herein are those of the authors and should not be interpreted as necessarily representing the official policies or endorsements, either expressed or implied, of NASA or the U.S. Government.

References

[1] Wise, K. A., Lavretsky, E., and Hovakimyan, N., "Adaptive Control of Flight: Theory, Applications, and Open Problems," *Proceedings of the American Control Conference*, Minneapolis, MN, 2006. doi:10.1109/ACC.2006.1657677

[2] Young, A., Cao, C., Hovakimyan, N., and Lavretsky, E., "An Adaptive Approach to Nonaffine Control Design for Aircraft Applications," Guidance, Navigation and Control Conference, AIAA Paper 2006-6343, Keystone, CO, 2006.

[3] Lavretsky, E., and Wise, K. A., "Adaptive Flight Control for Manned/Unmanned Military Aircraft," *Proceedings of the American Control Conference*, Portland, OR, 2005.

[4] Stevens, B., and Lewis, F., *Aircraft Control and Simulation*, Wiley, New York, 2003, pp. 206, 210, 339, 402.

[5] Lavretsky, E., "Robust Adaptive Inner-Loop Design for Vehicles with Uncertain Dynamics," *Proceedings of the American Control Conference*, Seattle, WA, 2008, pp. 2322–2327. doi:10.1109/ACC.2008.4586838

[6] Sanner, R., and Slotine, J.-J. E., "Gaussian Networks for Direct Adaptive Control," *IEEE Transactions on Neural Networks*, Vol. 3, No. 6, 1992, pp. 837–864. doi:10.1109/72.165588

[7] Kevorkian, J., and Cole, J. D., *Multiple Scale and Singular Perturbation Methods*, Applied Math Sciences 114, Springer–Verlag, New York, 1996, pp. 1–4.

[8] Narendra, K. S., and Annaswamy, A. M., *Stable Adaptive Systems*, Dover, New York, 2005, pp. 246–248.

[9] Ioannou, P. A., and Fidan, B., *Adaptive Control Tutorial*, Society for Industrial and Applied Mathematics, Philadelphia, 2006, pp. 31–32.

[10] Park, J., and Sandberg, I., "Universal Approximation Using Radial-Basis-Function Networks," *Neural Computation*, Vol. 3, No. 2, 1991, pp. 246–257. doi:10.1162/neco.1991.3.2.246

[11] Pomet, J. B., and Praly, L., "Adaptive Nonlinear Regulation: Estimation from the Lyapunov Equation," *IEEE Transactions on Automatic Control*, Vol. 37, No. 6, 1992, pp. 729–740. doi:10.1109/9.256328

[12] Khalil, H. K., *Nonlinear Systems*, Prentice–Hall, Upper Saddle River, NJ, 2002, p. 169.

[13] Lavretsky, E., Gadient, R., and Gregory, I., "Predictor-Based Model Reference Adaptive Control," *Journal of Guidance, Control, and Dynamics*, Vol. 33, No. 4, July–Aug. 2010, pp. 1195–1201. doi:10.2514/1.46849

[14] Lavretsky, E., "Combined/Composite Model Reference Adaptive Control," *IEEE Transactions on Automatic Control*, Vol. 54, No. 11, 2009, pp. 2692–2697. doi:10.1109/TAC.2009.2031580